Ab initio investigations of optical properties of the high-pressure phases of ZnO

Jian Sun and Hui-Tian Wang*
National Laboratory of Solid State Microstructures and Department of Physics, Nanjing University, Nanjing 210093, China

Julong He and Yongjun Tian
Key Laboratory of Metastable Materials Science and Technology, Yanshan University, Qinhuangdao 066004, China
(Received 22 November 2004; revised manuscript received 6 January 2005; published 31 March 2005)

We present a detailed investigation on optical properties of high-pressure phase ZnO in *B*1 (NaCl) and *B*2 (CsCl) structures, including dielectric function, refractive index, absorption, and electron energy-loss spectrum. Theoretical calculations are performed using the *ab initio* pseudopotential density functional method, in which we employ the Perdew-Burke-Eruzerhof form of the generalized gradient approximation available in the CASTEP code together with plane wave basis sets for expanding the periodic electron density. Both structures are optimized under the respective structural phase transition pressures; for the *B*1 structure it is 9 GPa, which has been verified to be in agreement with theory [Jaffe *et al.*, Phys. Rev. B **62**, 1660 (2000)] and experiment [Desgreniers, Phys. Rev. B **58**, 14102 (1998)], while for the *B*2 structure a transition pressure of 256 GPa is predicted in theory [Jaffe *et al.*, Phys. Rev. B **62**, 1660 (2000)]. We find that their electronic structures and optical properties under high pressure are quite different from those under ambient pressure.

DOI: 10.1103/PhysRevB.71.125132 PACS number(s): 78.20.Ci, 71.15.Mb, 61.50.Ks, 71.20.Nr

Recently, zinc oxide has attracted increasing interest because of its superior electronic, optical, and piezoelectric properties, leading to a wide range of applications such as transparent field-effect transistors, light-emitting diodes, ultraviolet nanolasers, photodetectors, solar cells, and surface acoustic wave devices.[1–3] Moreover, as a typical II-VI semiconductor and oxide, or just an example in mineralogy, the high-pressure behavior of ZnO has been a long-standing topic for geophysical and fundamental material physics reasons. Under ambient pressure, ZnO crystallizes the *B*4 (wurtzite) structure belonging to $P6_3mc$ space group. A great interest has been aroused in study on the high-pressure phases of ZnO both in experiments[4–6] and theories,[7,8] since Bates *et al.* discovered that the *B*4 phase ZnO could transform into the *B*1 (cubic NaCl) structure at a pressure of 9 GPa.[9] A recent calculation predicted that the sixfold-coordinated *B*1 ZnO could transform into the eightfold-coordinated *B*2 (cubic CsCl) structure under a pressure of 256 GPa.[10] Most of the works are devoted to the electronic properties,[11] elastic behaviors,[12–14] and lattice dynamics behaviors.[15–17] However, little is known about the optical properties of high-pressure phase ZnO, despite its significant importance for fundamental physics and potential applications of materials. For instance, using the optical measurements can directly characterize the structures of band. Very recently, the band gap measured from the optical absorption edge in the rocksalt phase was reported.[18] The results show an indirect band gap semiconductor with a band gap of 2.45 ± 0.15 eV.

In this article, we investigate the optical properties of the *B*1 and *B*2 phase ZnO under structural phase transition pressures of *B*4 to *B*1 and of *B*1 to *B*2, respectively. First, we carefully calculate the electronic structures, because the optical properties depend on both the interband and intraband transitions determined by the energy bands. Then, we discuss the optical properties, including the dielectric function, reflectivity, absorption, refractive index, and electron energy loss function and compare with those of the *B*4 structure under ambient pressure. Since the ionicity is an important factor to determine the structural phase transition pressure, we also discuss the charge and bond populations by the Mulliken population analysis.

The *ab initio* calculations described here are performed with the CASTEP code,[19] based on density functional theory (DFT) using Vanderbilt-type ultrasoft pseudopotentials[20] and a plane-wave expansion of the wave functions. We use the generalized gradient approximation (GGA) in the scheme of Perdew-Burke-Eruzerhof (PBE) to describe the exchange and correlation potential, since the GGA is more efficient to predict the phase transition pressure than the local-density approximation (LDA).[10] The structures are optimized under the structural phase transition pressures of 9 GPa for the *B*1 structure[4,10] and 256 GPa for the *B*2 structure.[10] To confirm the convergence of our calculations, we carefully investigate the dependences of the total energy on the cutoff energy and the *k*-point set mesh according to the Monkhorst-Pack grid. As an example, the results are plotted in Fig. 1, for the *B*4 ZnO. It can be seen that when the *k*-point set mesh is fixed in $12 \times 12 \times 7$, the change in total energy is less than 2 meV when the cutoff energy is higher than 700 eV; on the other hand, when the cutoff energy is fixed in 500 eV, the convergence in total energy is very well when the *k*-point set mesh is beyond $12 \times 12 \times 7$. In consideration of computational cost, we choose the cutoff energy to be in 700 eV, and the Brillouin-zone sampling mesh parameters for the *k*-point set are $12 \times 12 \times 7$ for the wurtzite *B*4 structure, $8 \times 8 \times 8$ for the rocksalt *B*1 structure and $13 \times 13 \times 13$ for the *B*2 structure, which make the separation of the reciprocal space to be less than 0.03 Å^{-1}.

As a common rule, under ambient pressure, the highly ionic materials have a tendency favoring the higher coordination structures (for instance, sixfold *B*1 and eightfold *B*2 structures with high symmetry), whereas the highly covalent materials favor the lower coordination structures (such as

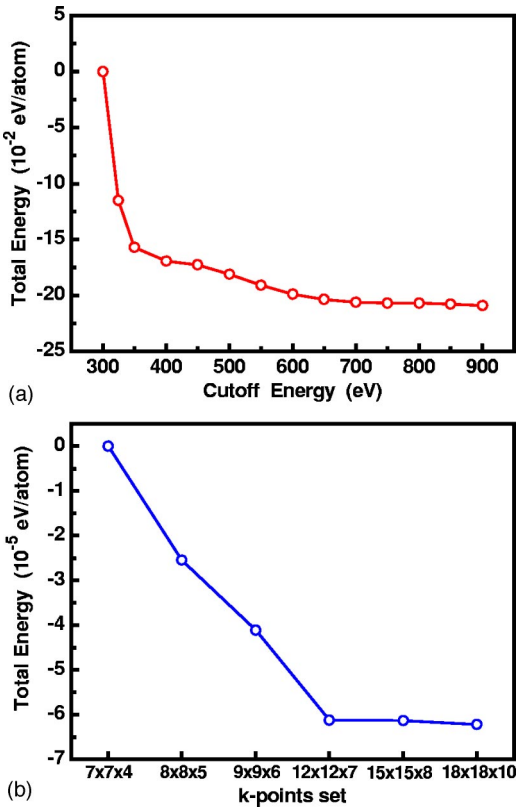

FIG. 1. (Color online) Convergences of the total energy of *B*4 ZnO at different computational parameters. (a) Total energy versus the cutoff energy for the *k*-point mesh of $12\times12\times7$. (b) Total energy versus the *k*-point set mesh for the cutoff energy of 500 eV.

fourfold zinc blende and *B*4 structures). Covalent materials could be transformed into the higher coordination phases through the high pressure method. Therefore, the structural phase transition pressure should be determined by the degree of ionicity being an important factor. For instance, the highly covalent semiconductor SiC starts to transform into *B*1 phase at a pressure of ~100 GPa,[21] while less covalent semiconductor GaAs starts to transform under a much lower pressure of ~17 GPa.[12] The high-ionicity materials such as MgO and CdO favor *B*1 structures in ambient pressure. Therefore, we will investigate the charge and chemical bonding of *B*4, *B*1, and *B*2 phase ZnO using Mulliken population analysis in detail. A technique for the projection of plane-wave states onto a linear combination of atomic orbitals basis set described in Ref. 22 is used to calculate the atomic charges and bond populations. It is well known that the absolute magnitudes of the atomic charges yield by the population analysis have little physical meaning, since they are highly sensitive to the atomic basis set. But we still can find some useful information by considering the relative values of Mulliken populations.

Table I shows the calculated charge transfer, bond lengths and bond populations of *B*4, *B*1, and *B*2 phase ZnO under different pressures. Compared with experimental value and previous calculations, the lattice parameters are also listed. Our results are a little smaller than the measured values[23] but better than the Hartree-Fock linear combination of atomic orbital (LCAO) results in Ref. 7 and the LDA results in Ref. 15. It can be found that the charge transfer is increased with the increase of the pressure. For the *B*4 structure, the charge transfer increase from 0.85 to 0.86 when the pressure is increased from 0 to 9 GPa, the bond length is compressed from 1.986 to 1.949 Å, and the bond population is also tone up from 0.40 to 0.42. When the *B*1 structure is compressed from 9 to 256 GPa, the charge transfer and the bond population are also increased while the bond length is reduced. This is easily understood that more electron cloud overlap together and more charge transfer from Zn atoms to O atoms when the bond length is compressed to shorter. It is interesting that the bond populations of the *B*4 and *B*1 structures under 9 GPa is all 0.42, implying that the ionicity of the Zn-O bonds in these two structures at this pressure is close.

TABLE I. Charge transfers, bond lengths, lattice parameters, and bond populations of *B*4, *B*1, and *B*2 phase ZnO under respective structural phase transition pressures.

Structure	Pressure (GPa)	Lattice constants (Å)		Charge transfer ($\|e\|$)	Bond length (Å)	Bond population
*B*4	0	$a=3.255$	$c=5.259$	0.85	1.986	0.40
		$a=3.2496(6)$	$c=5.2042(20)$[a]			
		$a=3.198$	$c=5.167$[b]			
		$a=3.290$	$c=5.241$[c]			
*B*4	9	$a=3.197$	$c=5.162$	0.86	1.949	0.42
*B*1	9	$a=4.237$		0.84	2.118	0.42
		$a=4.271$[a]				
		$a=4.225$[b]				
		$a=4.294$[c]				
*B*1	256	$a=3.650$		0.93	1.825	0.76
*B*2	256	$a=2.261$		0.88	1.958	0.16

[a]Experimental data from Ref. 23.
[b]Theoretical data from Ref. 15.
[c]Theoretical data from Ref. 7.

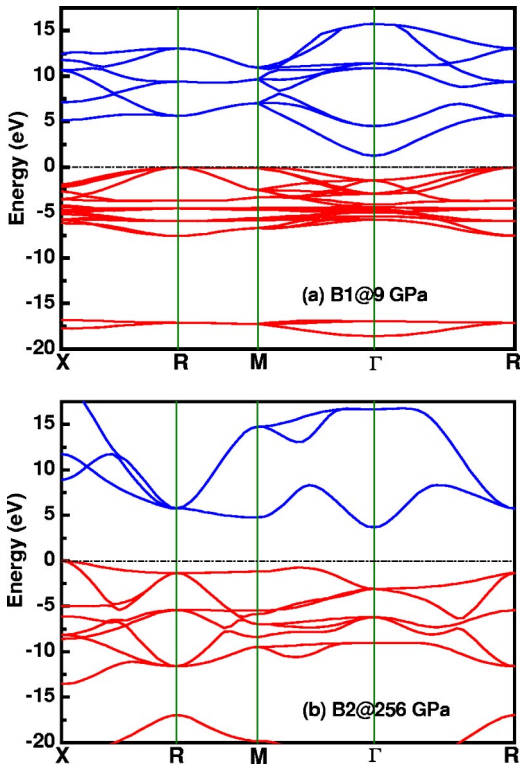

FIG. 2. (Color online) Bend structures: (a) for *B*1 ZnO under 9 GPa and (b) for *B*2 ZnO under 256 GPa.

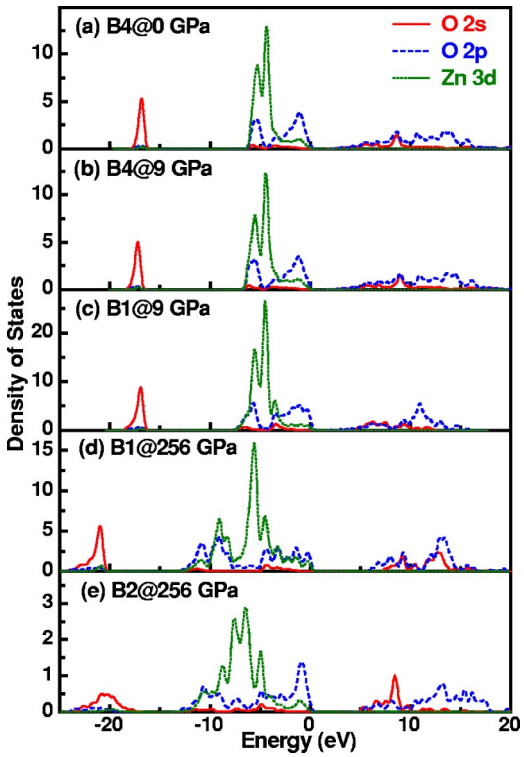

FIG. 3. (Color online) Density of states (DOS) for O 2*s*, O 2*p*, and Zn 3*d*. (a) *B*4 structure under ambient pressure, (b) *B*4 structure under 9 GPa, (c) *B*1 structure under 9 GPa, (d) *B*1 structure under 256 GPa, and (e) *B*2 structure under 256 GPa.

But the bond population of the *B*1 and *B*2 structures under 256 GPa is not so close.

From the band structure of the *B*1 ZnO shown in Fig. 2(a), we find that the direct band gap is ~2.73 eV at the highly symmetric Γ point and the smallest indirect band gap is ~1.29 eV in rocksalt ZnO, both are close to the respective values of 2.36 and 1.36 eV reported in Ref. 21 while have relatively large deviations from the corresponding values of 4.74 and 4.51 eV given in Ref. 11. A recent work[18] reported that rocksalt ZnO has an indirect band gap of 2.45±0.15 eV measured from optical absorption edge, but their theoretical result is also smaller than the measured one (1.1 eV). So our results may give some evidence that the GGA results usually underestimate the band gap than the experimental values, moreover, the rocksalt ZnO should be an indirect band gap semiconductor and the actual value is about 2.5 eV. The band structure of the *B*2 ZnO shown in Fig. 2(b) indicates that it has a direct band gap of ~6.75 eV at the Γ point, which is much larger than the smallest indirect band gap of ~3.68 eV. However so far there are no experimental data available that could verify these calculated results.

The density of states (DOS) of the *B*4, *B*1, and *B*2 structures under their phase transition pressure are plotted in Fig. 3. We find that when *B*4 ZnO is compressed, the peaks of DOS in the valence bands have a tendency shifting to the lower energy. For instance, for the Zn 3*d* orbitals the two peaks are shifted from −4.39 and −5.32 eV to −4.47 and −5.57 eV, respectively; for the O 2*s* orbitals the peak from −16.88 to −17.24 eV; and for the O 2*p* orbitals from −1.11 and −5.45 eV to −1.20 and −5.57 eV, respectively. In the *B*1 structure under transition pressure (9 GPa), the peaks of the O 2*p* and O 2*s* orbitals are slightly broadened and the peaks of the Zn 3*d* and O 2*s* orbitals are enhanced, the peaks' positions are more close to the *B*4 structure under 9 GPa. For *B*1 structures, the shift of the peaks is more obvious since the pressure change is larger. The peaks from ZnO 3*d* are broad much and the secondary highest peak becomes the highest one at −5.61 eV. The peaks of *B*2 structure under 256 GPa are broader and the height becomes small. This is understood that the overlap of the bonds is increased and the hybridization is changed.

From the band structures of high pressure phase ZnO, we can find the maxima of the valence bands are flat, indicating that they have large hole effective masses, which should result in some unusual transport properties for *p*-type semiconductor. Moreover, the structural phase transition (the change in symmetry) originating from the pressure may lead to different selection rules, which together with the altered density and band hybridization, may bring some unusual optical properties and potential applications.[24] This is the main reason why we discuss the optical properties of high-pressure phase ZnO in detail.

It is well known that the interaction of a photon with the electrons in the system can be described in terms of time-dependent perturbations of the ground-state electronic states. Transitions between occupied and unoccupied states, including plasmons and single particle excitations, are caused by the electric field of the photon. The spectra resulting from these excitations can be described as a joint density of states between the valence and conduction bands. The imaginary

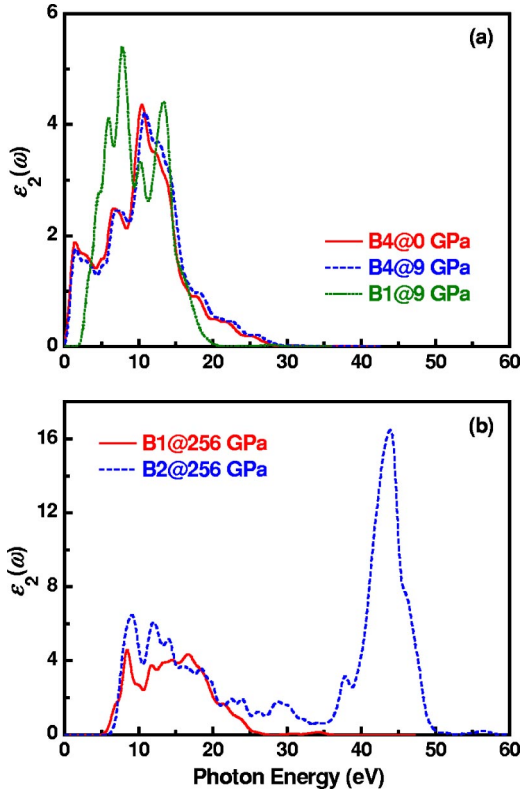

FIG. 4. (Color online) Imaginary part of dielectric function $\varepsilon_2(\omega)$. (a) $B4$ structure under ambient pressure, $B4$ structure under 9 GPa, and $B1$ structure under 9 GPa and (b) $B1$ structure and $B2$ structure under 256 GPa.

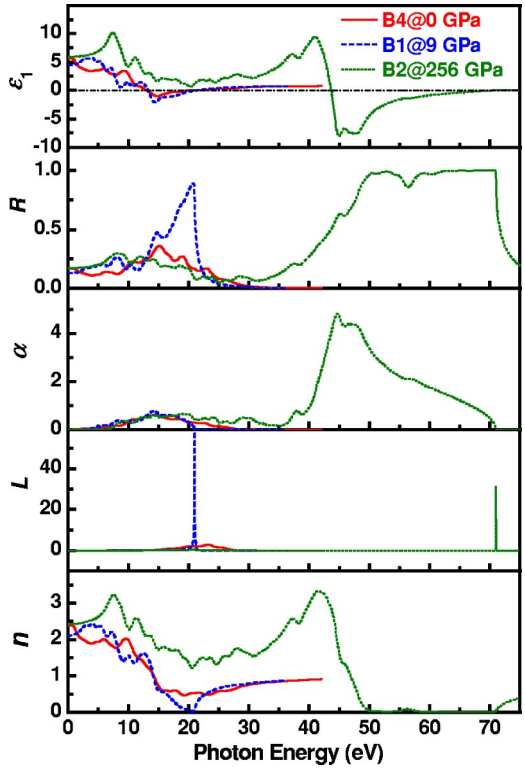

FIG. 5. (Color online) Real part of the dielectric function $\varepsilon_1(\omega)$, reflectivity $R(\omega)$, absorption coefficient $\alpha(\omega)$, refractive index $n(\omega)$, and electron energy-loss function $L(\omega)$ of $B4$ structure under ambient pressure, $B1$ structure under 9 GPa, and $B2$ structure under 256 GPa.

part $\varepsilon_2(\omega)$ of the dielectric function could be calculated from the momentum matrix elements between the occupied and unoccupied wave functions within the selection rules, and the real part $\varepsilon_1(\omega)$ of dielectric function can be evaluated from imaginary part $\varepsilon_2(\omega)$ by Kramer-Kronig relationship. All the other optical constants can be derived from $\varepsilon_1(\omega)$ and $\varepsilon_2(\omega)$, such as reflectivity $R(\omega)$, absorption coefficient $\alpha(\omega)$, refractive index $n(\omega)$, and energy-loss spectrum $L(\omega)$

$$R(\omega) = \left| \frac{\sqrt{\varepsilon_1(\omega) + j\varepsilon_2(\omega)} - 1}{\sqrt{\varepsilon_1(\omega) + j\varepsilon_2(\omega)} + 1} \right|^2, \quad (1)$$

$$\alpha(\omega) = \sqrt{2}\omega[\sqrt{\varepsilon_1^2(\omega) + \varepsilon_2^2(\omega)} - \varepsilon_1(\omega)]^{1/2}, \quad (2)$$

$$n(\omega) = [\sqrt{\varepsilon_1^2(\omega) + \varepsilon_2^2(\omega)} + \varepsilon_1(\omega)]^{1/2}/\sqrt{2}, \quad (3)$$

$$L(\omega) = \varepsilon_2(\omega)/[\varepsilon_1^2(\omega) + \varepsilon_2^2(\omega)]. \quad (4)$$

It is noted that $R(\omega)$ is the reflectivity in the case when assuming orientation of the crystal surface parallel to the optical axis.[25] As we know, the imaginary part of dielectric function $\varepsilon_2(\omega)$ is the pandect of the optical properties for any materials, so we plot the imaginary parts of the dielectric functions of the $B4$ structure under ambient pressure, the $B4$ and $B1$ structures under phase transition pressure (9 GPa) in Fig. 4(a). For the $B4$ structure, there are three main peaks in $\varepsilon_2(\omega)$. For the $B4$ structure, the line shape of $\varepsilon_2(\omega)$ is almost unchanged while there is a little shift forward high-energy region (blue shift), when it is compressed to 9 GPa. The peak at around 1.4 eV mainly comes from the electron transition between the O $2p$ and Zn $4s$ orbitals. The transition between the Zn $3d$ and O $2p$ orbitals may lead to the peak at about 6.7 eV. And the peak at 10.4 eV is mainly derived from the transition between the Zn $3d$ and O $2s$ orbitals. For the $B1$ structure under 9 GPa, the profile is not so broad as that of the $B4$ structure. The peaks mainly come from the electron transition between the Zn $3d$ and O $2p$ orbitals. For the $B1$ and $B2$ structures under 256 GPa, $\varepsilon_2(\omega)$ are plotted in Fig. 4(b). For the $B1$ structure, the peaks shift to high-energy region (blue shift) than that under 9 GPa. For the $B2$ structure, there is a remarkable high peak at about 44 eV, which indicates that the $B2$ structure under 256 GPa should have some interesting characters in the high-energy range.

The real part of dielectric function $\varepsilon_1(\omega)$, the reflectivity $R(\omega)$, the absorption coefficient $\alpha_2(\omega)$, the refractive index $n(\omega)$, and the electron energy loss function $L(\omega)$ of the $B4$ structure under ambient pressure, the $B1$ structure under 9 GPa and the $B2$ structure under 256 GPa are plotted in Fig. 5. Because the $B1$ and $B2$ structures are optically isotropic while the $B4$ structure is optically anisotropic we only give the optical properties in the case of the polycrystalline, in which the optical properties are averaged over all polarizations possible, thereby imitating an experiment on a polycrystalline sample. The absorption band of the $B1$ structure under 9 GPa is narrower than that of the $B4$ under ambient

pressure; the former is about 0–22.0 eV while the latter is about 0–30.0 eV. In contrast, the *B*2 structure has a more broad absorption band covering from 0 to 71.0 eV and has a strong peak at around 44.6 eV. In the dispersion curve of the refractive index of the *B*2 structure, there are two remarkable peaks at 7.5 and 41.5 eV. $L(\omega)$ is also an important factor describing the energy loss of a fast electron traversing in a material. The peaks in $L(\omega)$ spectra represent the characteristic associated with the plasma resonance and the corresponding frequency is the so-called plasma frequency, above which the material exhibits the dielectric behavior $[\varepsilon_1(\omega)>0]$ while below which the material behaves the metallic property $[\varepsilon_1(\omega)<0]$. That is to say, the positions of peaks in $L(\omega)$ spectra indicate also the point of transition from the metallic property to the dielectric property for a material. In addition the peaks of $L(\omega)$ also correspond to the trailing edges in the reflection spectra, for instance, the peak of $L(\omega)$ for the *B*1 structure is at 21.0 eV corresponding to the abrupt reduction of $R(\omega)$, and the corresponding peak of $L(\omega)$ for the *B*2 structure appears at about 71.0 eV, in which the reflectivity for the *B*2 structure is also sharply reduced.

In conclusion, the electronic structures and optical properties of ZnO in the *B*1 (NaCl) and *B*2 (CsCl) structures under their structural phase transition pressures were investigated by *ab initio* ultrasoft pseudopotential density functional method in detail. The dielectric function and the optical properties such as reflectivity, absorption coefficient, refractive index, and electron energy-loss function were presented in a wide energy range. The band structure of the *B*1 phase is well agreed with previous literature. The results of optical properties indicated that the high-pressure phases ZnO have remarkable characters at the high-energy regime and may lead to some potential applications. In addition it is of great importance for understanding of the high-pressure behaviors of wide band gap semiconductors.

This work was partially supported by National Natural Science Foundation of China (Grant Nos. 10325417, 90101030, and 50372055).

*Electronic address: htwang@nju.edu.cn

[1] K. Nomura, H. Ohta, K. Ueda, T. Kamiya, M. Hirano, and H. Hosono, Science **300**, 1269 (2003).
[2] M. H. Huang, S. Mao, H. Feick, H. Yan, Y. Wu, H. Kind, E. Weber, R. Russo, and P. Yang, Science **292**, 1897 (2001).
[3] C. T. Lee, Y. K. Su, and H. M. Wang, Thin Solid Films **150**, 283 (1987).
[4] S. Desgreniers, Phys. Rev. B **58**, 14102 (1998).
[5] J. M. Recio, M. A. Blanco, V. Luana, R. Pandey, L. Gerward, and J. S. Olsen, Phys. Rev. B **58**, 8949 (1998).
[6] Z. Y. Wu, Z. X. Bao, X. P. Zou, D. S. Tang, C. X. Liu, J. H. Dai, S. S. Xie, Q. S. Li, Z. X. Shen, and B. S. Zou, Mater. Sci. Technol. **19**, 981 (2003).
[7] J. E. Jaffe and A. C. Hess, Phys. Rev. B **48**, 7903 (1993).
[8] S. Limpijumnong and S. Jungthawan, Phys. Rev. B **70**, 054104 (2004).
[9] C. H. Bates, W. B. White, and R. Roy, Science **137**, 993 (1962).
[10] J. E. Jaffe, J. A. Snyder, Z. Lin, and A. C. Hess, Phys. Rev. B **62**, 1660 (2000).
[11] H. Q. Ni, Y. F. Lu, and Z. M. Ren, J. Appl. Phys. **91**, 1339 (2002).
[12] R. K. Singh and Sadhna Singh, Phys. Rev. B **39**, 671 (1989).
[13] J. Zhang and R. C. Liebermann, Europhys. Lett. **51**, 268 (2000).
[14] R. Ahuja, L. Fast, O. Eriksson, J. M. Wills, and B. Johansson, J. Appl. Phys. **83**, 8065 (1998).
[15] J. Serrano, A. H. Romero, F. J. Manjon, R. Lauck, M. Cardona, and A. Rubio, Phys. Rev. B **69**, 094306 (2004).
[16] F. Decremps, J. Pellicer-Porres, A. M. Saitta, J. Chervin, and A. Polian, Phys. Rev. B **65**, 092101 (2002).
[17] F. J. Manjon, K. Syassen, and R. Lauck, High Press. Res. **22**, 299 (2002).
[18] A. Segura, J. A. Sans, F. J. Manjon, A. Munoz, and M. J. Herrera-Cabrera, Appl. Phys. Lett. **83**, 278 (2003).
[19] M. Segall, P. Lindan, M. Probert, C. Pickard, P. Hasnip, S. Clark, and M. Payne, J. Phys.: Condens. Matter **14**, 2717 (2002).
[20] D. Vanderbilt, Phys. Rev. B **41**, 7892 (1990).
[21] M. Yoshida, A. Onodera, M. Ueno, K. Takemura, and O. Shimomura, Phys. Rev. B **48**, 10587 (1993).
[22] D. Sanchez-Portal, E. Artacho, and J. M. Soler, Solid State Commun. **95**, 685 (1995); M. D. Segall, R. Shah, C. J. Pickard, and M. C. Payne, Phys. Rev. B **54**, 16317 (1996).
[23] H. Karzel, W. Potzel, M. Köfferlein, W. Schiessl, M. Steiner, U. Hiller, G. M. Kalvius, D. W. Mitchell, T. P. Das, P. Blaha, K. Schwarz, and M. P. Pasternak, Phys. Rev. B **53**, 11425 (1996).
[24] J. E. Jaffe, R. Pandey, and A. B. Kunz, Phys. Rev. B **43**, 14030 (1991).
[25] S. Saha and T. P. Sinha, Phys. Rev. B **62**, 8828 (2000); M. Q. Cai, Z. Yin, and M. S. Zhang, Appl. Phys. Lett. **83**, 2805 (2003).